euronoise 2021
25th to 27th of October
Madeira, Portugal - online

Reduction of low-frequency vibration of joist floor structures by multiple dynamic vibration absorbers: comparison of experimental and computational results

Yi Qin [1], Jin Jack Tan[1,2], Maarten Hornikx [1]

[1] Department of the Built Environment, Eindhoven University of Technology, Eindhoven, the Netherlands
[2] Sorama BV, Eindhoven, the Netherlands

Abstract
Typical solutions to reduce excessive floor vibration and its radiated sound are increasing mass, stiffening the structure, or adding a floating floor. However, these methods may not be effective on lightweight floors in reducing low-frequency impact sound.
The use of dynamic vibration absorbers is an attractive approach to reduce the response of the structure at its natural frequency. For studying the effect of multiple dynamic vibration absorbers and designing optimal solutions for various configurations, an efficient modelling approach is desired.
A model is proposed for this purpose that utilizes the thin plate theory for the floor and the Timoshenko beam theory for the joists. In addition to the joists' bending motion, the model has also included the joists' rotation and approximates the plate-beam interface connection condition. To verify the appropriateness of the model, measurements on a scaled joist floor structure have been carried out. The joist structure in the test is made of medium-density fiberboards, while the absorbers are made of steel springs and mass blocks. A good agreement of the impact of vibration absorbers is shown in the modal assurance criterion (MAC) and the comparison of the transfer functions.

Keywords: vibration, joist floor, vibration absorber, low frequency, experiment.

1 Introduction

Annoyance due to impact sound from floors is related to the excessive vibration of the floor. For the sake of comfort and health, people's exposure to impact noise and floor vibration should be avoided [1, 2]. To achieve this goal, an adequate vibration control to the floor is needed.

Typical solutions to reduce the floor vibration are to redesign and modify the floor systems by increasing the thickness and thereby the mass, stiffening the structure, and adding an elastically-supported floor covering [3, 4]. The first two methods modify the dynamics of the system such that the excitation is less effective on floor responses and the dominant floor natural frequencies are shifted away from the most problematic frequency range, while the last method decouples the vibrations from the top floor to the base structure thereby reducing the radiated sound from the floor. However, improving the stiffness is hard to implement on lightweight floors. The approach using a floating floor or additional masses produces drawbacks such as the weight increase and lower fundamental frequencies, leading to potential worse vibration conditions in the low frequency range [4, 5].

The idea of a passive vibration absorber emerges in structural engineering applications since its introduction in 1911 by [6]. By tuning the spring, mass, and damping, the natural mode of a single degree of freedom (SDOF) the host

system can be effectively suppressed, such that the structural vibration can be reduced (Figure 1). Vibration absorbers can be installed more cheaply than structural stiffening and are sometimes the only approach of vibration control in existing structures [7].

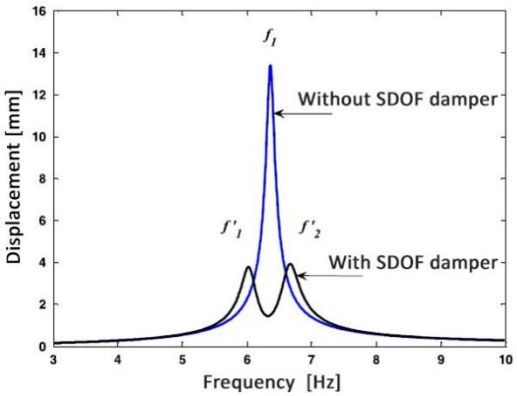

Figure 1 – Example of frequency response curves of a SDOF vibration absorber.

In the last two decades, applying vibration absorbers to control the floor vibrations have been popularly studied theoretically. By assuming the floor and the absorber as single-mode systems, the vibration of the coupled structure is simplified as a two-degree-of-freedom system [8, 9]. This simple method allows an analysis on suppressing the fundamental mode of a floor structure. For controlling the vibration of a more complex floor by absorbers, using FEM to solve the governing partial differential equations does provide more detailed simulations. However, the calculation may be tedious due to complex and detailed floor geometries [10, 11]. Additionally, analytical models of rectangular plates with classical boundary conditions provide insight into the low frequency bending vibrations and may be easily coupled with the spring-mass models. Therefore, they are frequently applied in parametric studies and optimizations of the absorber on a plate [10, 12, 13, and 14].

In contrast, in only a few studies measurements of absorbers have been conducted [15, 16], and even fewer on measurements of absorbers applied to floor structures [7]. Also, most of these experiments were carried out for the applications of a single absorber rather than distributed multiple absorbers.

In this paper, the effect of multiple vibration absorbers on the vibration of a lightweight joist floor is investigated. An experiment was conducted on a scaled joist structure with absorbers made of steel springs and mass blocks. Low-frequency vibration results are compared with those calculated by an analytical model based on a modal superposition method. The aim of this research is to evaluate the applicability of the analytical model in predicting the effect of the multiple vibration absorbers on the vibration field of joist floors.

The paper is organized as follows: Section 2 presents the setup of the experiment and test results, and Section 3 presents the formulation and validation of the analytical prediction model. Section 4 presents the results and comparisons are made between the predicted and measured vibration results. In Sections 5 and 6, some discussions and conclusions are given.

2 Experimental analysis

The experiment took place in the acoustics laboratory of Eindhoven University of Technology. Figure 2 shows the scaled joist floor structure used in this research. The basic structure is fabricated by a 1m x 1m x 9mm medium-density-fibreboard (MDF) plate supported by 7 MDF beams with a cross section of 22 x 70mm. The

beams are evenly spaced in *x*-direction with a distance of around 135mm. Each beam is connected to the plate by 9 screws (spaced 135mm from each other).

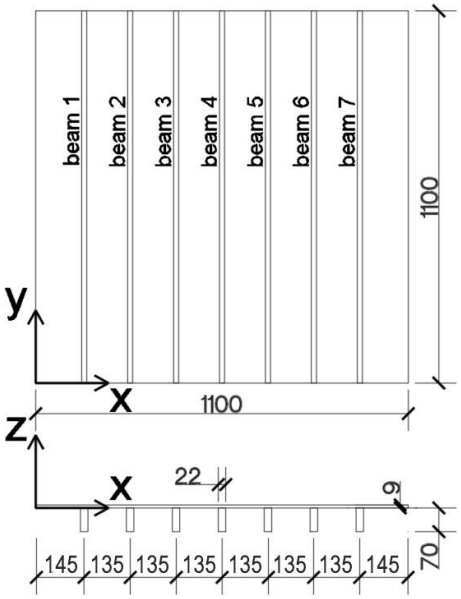

Figure 2 – Top and front view of the scaled joist floor. The dimensions are in [mm].

In the experiment, the structure was suspended by elastic ropes so as to obtain freely-supported boundary conditions. The normal vibrations of the top plate, excited by impact hammer BK 8202, are measured at 17x9 positions by accelerometers PCB 333B30. The signals were captured by a National-Instruments acquisition system (NI 9234 and cDAQ-9178) for 7 seconds with a sampling frequency of 51200Hz, and then the fast Fourier transform (FFT) was applied in Matlab for a frequency range up to 25.6 kHz.

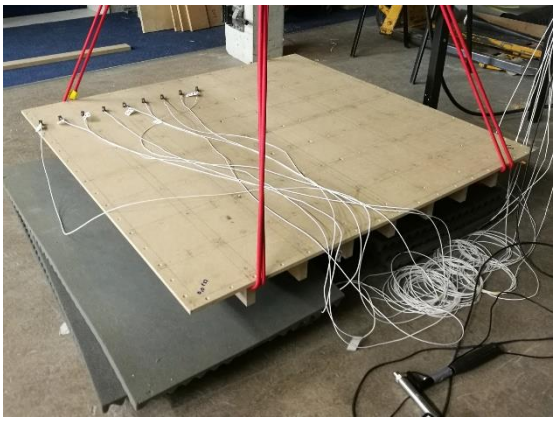

Figure 3 – Setup of the experiment on the joist structure.

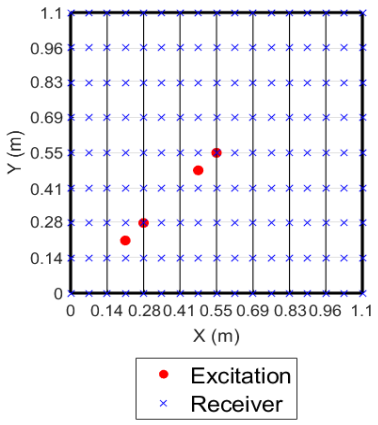

Figure 4 – Locations of the force excitation and accelerometers.

2.1 Mechanical properties of the wooden components

The densities of the wooden components were determined by weighting them separately. The Young's moduli of both plate and beams are assumed to be homogeneous and were obtained by performing dynamic vibration

tests. In the measurements, the components were placed on a soft porous material to obtain a freely-supported condition, as shown in Figures 4 and 5. A 0.25 Poisson's ratio borrowed from [17, 18] is given to all the MDF components. The Young's moduli of the plate and beams were calibrated by using finite element models solving the equations of linear elasticity. The values of the Young's moduli are finally determined by matching the simulated and measured natural frequencies of the first bending modes (the 22.3Hz mode for the plate and the around 120Hz mode for the beams). The loss factors were extracted from the measured transfer functions by using the half-power bandwidth approach [19, 20]. The properties of the wooden components are listed in Table 1.

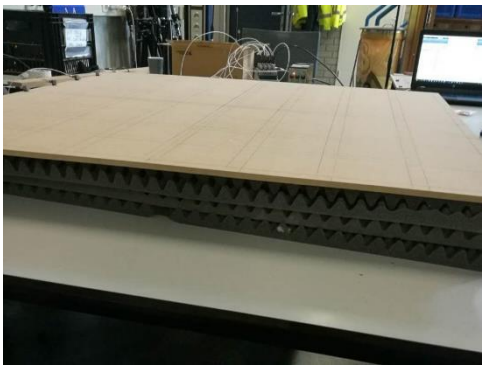

Figure 5 – Measurement setup of the dynamic property test on the MDF plate.

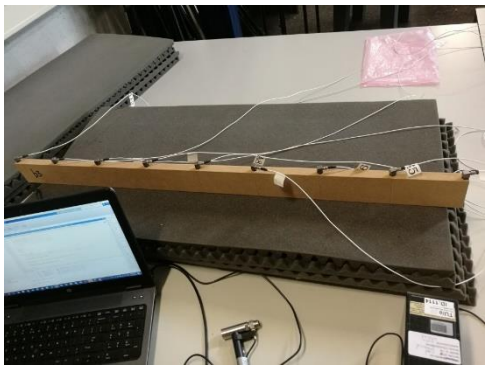

Figure 6 – Measurement setup of the dynamic property test on the MDF beam.

Table 1 – Mechanical properties of the wooden components identified by dynamic vibration tests

	Young's modulus GPa	Density kg/m3	Loss factor
Plate	3.1	669.6	0.052
Beam 1	1.9	583.2	0.045
Beam 2	2.1	565.2	0.039
Beam 3	2.1	559.2	0.038
Beam 4	2.1	571.2	0.081
Beam 5	2.1	577.2	0.078
Beam 6	2.4	589.2	0.088
Beam 7	2.1	577.2	0.055

2.2 Design and fabrication of the vibration absorber

Eight vibration absorbers are used in the measurement in total. Each absorber consists of three parts welded to each other: a steel mass block, a steel coil spring, and a hex nut used to connect with the joist structure (Figure 7).

The natural frequencies of the absorbers are designed to be 70Hz, corresponding to the bending modes of the joist structure at that frequency. The absorbers are characterized by spring constant k_a and mass m_a. Firstly, the dimensions of the coil springs were calculated by

$$k_a = \frac{Gd^4}{8nD^3} \tag{1}$$

where G is the transverse elastic modulus of the spring material, d is the wire diameter, n is the number of the active coils and D is the mean coil diameter (outer diameter - wire diameter). Then, by changing m_a, the natural frequency of the absorbers can be tuned to the desired frequency.

A finite element model of the vibration absorber was made in COMSOL multi-physics. The model solves the linear elasticity equation and assumes the materials are homogeneous. The dimensions of coil spring (D, d and n) are given as 12mm, 2mm and 6, and the dimension of the block is 30 x 30 x 19mm. The Young's modulus, Poisson's ratio and the density of steel are given to the whole absorber as 205Gpa, 0.28, and 7850kg/m^3. The top surface of the hex nut is set to be fixed and the low-frequency modal patterns of the vibration absorber are analysed.

The desired 70 Hz resonance in the vertical direction was found in the finite element model, as shown in Figure 8. However, except for the resonance around 70 Hz, some mode types have been observed in the FE model, such as a rotational mode at 33.5 Hz and two swing modes, axial and diagonal, at 13.7 and 115Hz.

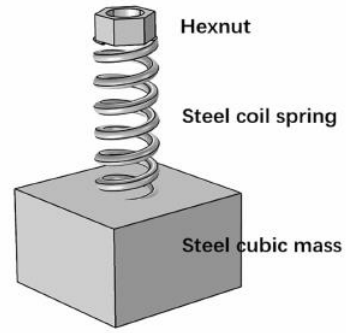

Figure 7 – Setup of a single vibration absorber.

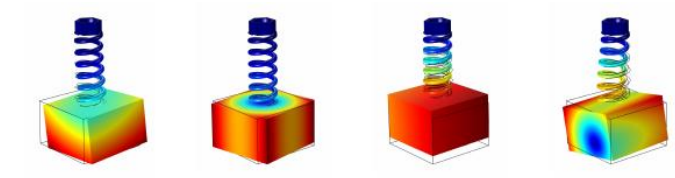

Figure 8 – Natural modes of the vibration absorber simulated by COSMOL.

These modes are also observed in an impact-response test on the fabricated vibration absorber. In the test, the vibration absorber is fixed on the hex nut by a pressure clamp. An accelerometer is attached on the bottom surface of the mass block to measure the vertical vibrations excited by the hammer impacts, as shown in Figure 9. In the result, a peak was observed around 70 Hz, which represents the designed mode of the absorber (Figure 10); two other peaks were found at 14 and 115 Hz, which are most likely due to the axial and diagonal swing modes. The rotational mode is not clearly shown in the figure, as the horizontal movements cannot be collected by the used sensor.

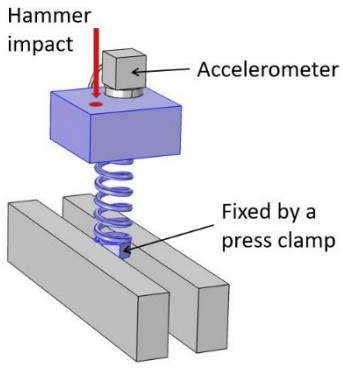

Figure 9 – Measurement setup of the absorber's natural frequencies.

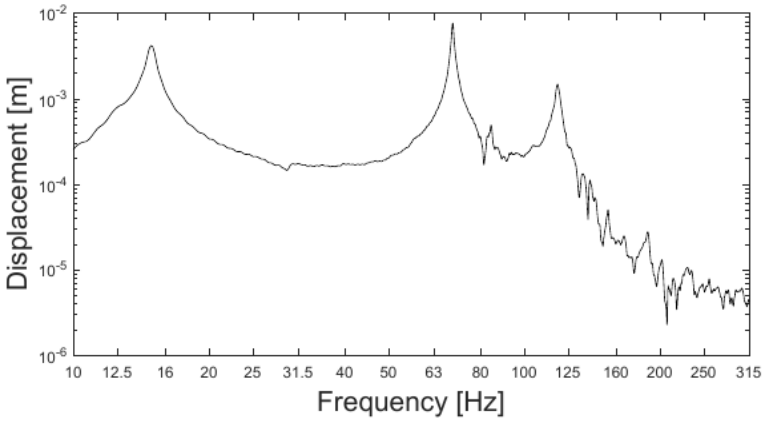

Figure 10 – Measured frequency response of the vibration absorber system.

To achieve an obvious effect on the floor's response, the vibration absorbers were installed in the area having the highest displacement at the target frequency. As shown in Figure 11, the structure has a high displacement along the central beam at the 70Hz mode. Therefore, the absorbers are allocated and distributed in the area along the central beam (Figure 12). The averaged values of the parameters measured from 8 absorbers are listed in Table 2.

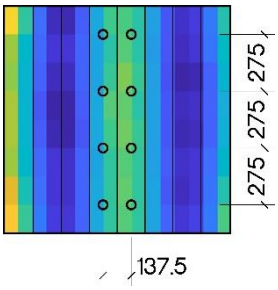

Figure 11 – 70Hz Mode shape of the structure and positions of the vibration absorbers.

Figure 12 – Setup of the vibration absorbers installed on the joist structure.

Table 2 – Mechanical properties of the wooden components identified by dynamic vibration tests

Components	Spring constant k_a, N/m	Mass m_a, kg	Loss factor η_a	Natural frequency, f_a, Hz
Absorber	2.55e4	0.121	0.01	73

3 Numerical analysis

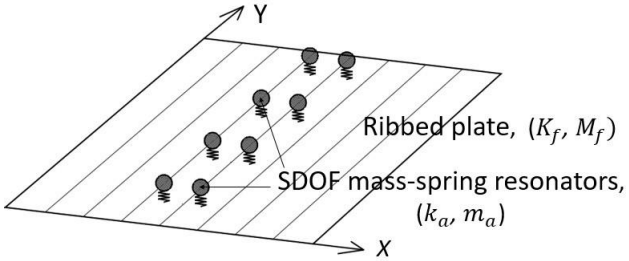

Figure 13 – Schematic representation of the joist structure with SDOF vibration absorbers.

Figure 13 illustrates the analytical model of the joist floor with the vibration absorbers. The structure is considered as a thin ribbed plate lying in the x–y plane, and the vibration absorbers are sketched as SDOF mass-spring resonators. The prediction model of the joist structure is based on the modal superposition model.

3.1 Analytical model of the joist floor with free boundary condition

To calculate the vibration displacement of the joist floor structure, firstly, the coefficients of the modal displacement of the structure are computed by

$$(\mathbf{K_{floor}} - \mathbf{M_{floor}}\omega^2)\mathbf{u_{floor}} = \mathbf{F} \quad (2)$$

where $\mathbf{K}_{\mathbf{floor}}$ and $\mathbf{M}_{\mathbf{floor}}$ are the stiffness and mass matrices of the plate. $\mathbf{u}_{\mathbf{floor}}$ is the coefficient vector of the modal displacement. The vibration displacement of the joist floor is calculated by

$$w_{floor}(x,y) = \sum_{n=1}^{N}\sum_{m=1}^{M} u_{floor}(m,n)\phi_m(x)\psi_n(y) \tag{3}$$

in which ϕ_m and ψ_m are the mode shape functions of the floor mode (m,n) along x and y directions.

For the joist floor, the bending motion of the plate are combined with the bending and torsional motions of the beams by defining the $\mathbf{K}_{\mathbf{floor}}$ and $\mathbf{M}_{\mathbf{floor}}$ as

$$\mathbf{K_{floor}} = \mathbf{K_p} + \mathbf{K_{b,1}} + \mathbf{K_{b,2}} \tag{4}$$

$$\mathbf{M_{floor}} = \mathbf{M_p} + \mathbf{M_{b,1}} + \mathbf{M_{b,2}} \tag{5}$$

where $\mathbf{K_p}$ and $\mathbf{M_p}$ are the stiffness and mass matrices of the plate, $\mathbf{K_{b,1}}$, $\mathbf{K_{b,2}}$, $\mathbf{M_{b,1}}$, $\mathbf{M_{b,2}}$ are the stiffness and mass matrices of the beams for the bending (index 1) and torsional motion (index 2).

The matrices $\mathbf{K_p}$ and $\mathbf{M_p}$ of a free-free rectangular thin plate are given by [23], the bending stiffness matrix $\mathbf{K_{b,1}}$ and mass matrices $\mathbf{M_{b,1}}$ of S beams are defined as [23], and the torsional stiffness matrix $\mathbf{K_{b,2}}$ and mass matrices $\mathbf{M_{b,2}}$ are defined as [24]

3.1.1 Mode shape function for a plate with free boundary condition on four edges

To be consistent with the measurement setup, the model of the joist floor contains free boundary conditions for all edges of the plate. The mode shape functions of the plate can be approximated by [21, 22]

$$\phi_m(x) = \sqrt{\frac{2}{l_x}}\varphi_f(x), \quad \psi_n(y) = \sqrt{\frac{2}{l_y}}\varphi_f(y) \tag{6}$$

in which φ_f is the mode shape function of the beam and the subscript f denotes the free boundary condition. The function φ_f is described as

$$\begin{aligned}
&\varphi_{f,0}(x) = \sqrt{1/2},\\
&\varphi_{f,1}(x) = \sqrt{3/2}\left(1 - \frac{2x}{l_x}\right),\\
&\varphi_{f,2,4,6\ldots}(x) = cos\left[k_i\left(\frac{x}{l_x} - \frac{1}{2}\right)\right] + a_i cosh\left[k_i\left(\frac{x}{l_x} - \frac{1}{2}\right)\right],\\
&\varphi_{f,3,5,7\ldots}(x) = sin\left[k'_i\left(\frac{x}{l_x} - \frac{1}{2}\right)\right] + a'_i sinh\left[k'_i\left(\frac{x}{l_x} - \frac{1}{2}\right)\right],
\end{aligned} \tag{7}$$

where

$$a_i = \frac{sin(k_i/2)}{sinh(k_i/2)}, \qquad a'_i = \frac{sin(k'_i/2)}{sinh(k'_i/2)} \tag{8}$$

and the constants k_i and k'_i are given in Table 3.

Table 3 – Constants k_i and k'_i for Equation 7, r=3,4,5...

k_2=4.7300	k'_3 =7.8532
k_4=10.9956	k'_5 =14.1372
$k_{6,8,10\ldots}$ =(4r − 1) π/2	$k'_{7,9,11\ldots}$ =(4r + 1) π/2

3.1.2 Interface connection between plate and beams

The analytical model assumes the beams to bend along their neutral planes and the displacements on their neutral planes are coupled with that of the plate, as shown in Figure 14(a). However, in a real joist floor, the plate and the beams are connected on their physical interfaces, as shown in Figure 14(b). This type of connection will lead to an unevenly distributed stress on the cross section when the bending happens in the structure, thus an up-shift of bending axis of the beam has to be accounted for in the bending motion [25].

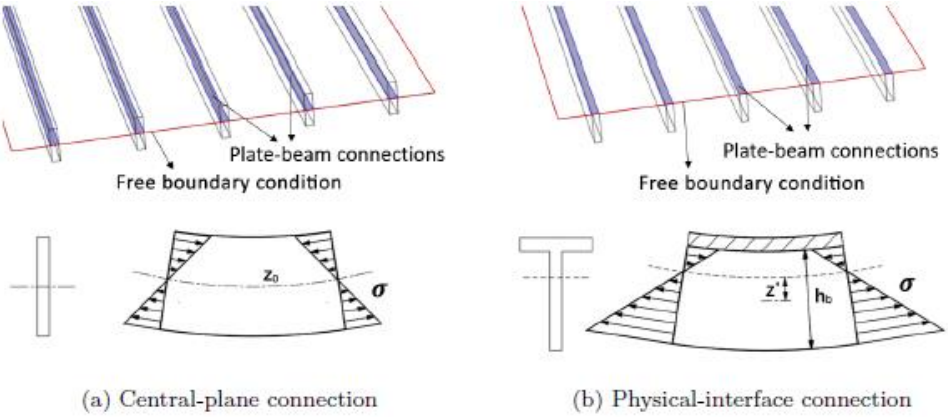

Figure 14 – Plate-beam connections and the neutral plane of the joist structure.

To approximate the effect of the interface connections, a revised second moment of inertia of the beam, I'_b, with a shifted bending axis value, z', is introduced into the model based on the parallel axis theorem [26]. The equation for the revised second moment of inertia is given by

$$I'_b = I_b + A_b z'^2 \tag{9}$$

In this research, the plate and the beams are firmly connected by the screws. A $z'=0.5h_b$ is applied for the bending modes n=3,4…N of the beams, where h_b is the height of the beam. The original I_b is still used for the first two rigid-body-motion modes (n=1,2).

3.2 Numerical validation of the analytical model by finite element models

The analytical model was validated by comparing with a finite element model made in the COMSOL multi-physics software. The model was made of a 2D plate solving the Mindlin plate theory and 3D beams solving linear elasticity equations. In the analytical model, both the bending waves and the torsional waves of the beams were considered ($\mathbf{K_{floor}}=\mathbf{K_p}+\mathbf{K_{b,1}}+\mathbf{K_{b,2}}$ and $\mathbf{M_{floor}}=\mathbf{M_p}+\mathbf{M_{b,1}}+\mathbf{M_{b,2}}$), and the beam's second moment of inertia was calculated by Equation 24 with $z'=0.5h_b$ for the modes n>3.

The floor structure was assumed to be excited simultaneously at 2 impact positions, and the mobility at 17 x 9 receiving positions were calculated and root-mean-squared for the comparison, see Figure 15. Two results show a generally good agreement in Figure 16.

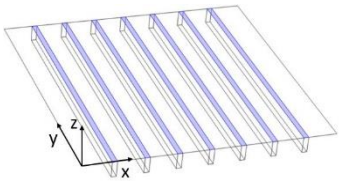

Figure 15 – Geometry of the finite element model.

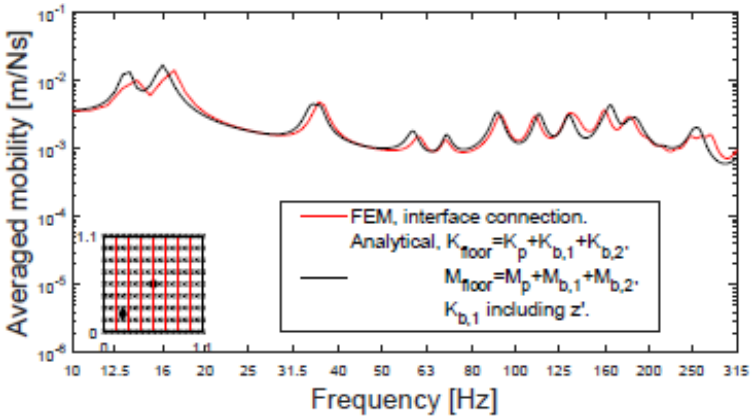

Figure 16 – Result of the averaged mobility. The small map shows the impact (dots) and the receiving position (cross signs).

3.3 Modelling the joist floor with vibration absorbers

The vibration absorbers are modelled as SDOF mass-spring systems. The displacements of the absorbers, $w_{a.r}$, are coupled with the motion of joist structure $w_{floor,r}$ at the attaching positions ($x_{a,r}$, $y_{a,r}$). The displacement of the floor at the position of the absorber r can be represented by

$$w_{floor,r} = \sum_{n=1}^{N}\sum_{m=1}^{M} u_{floor}(m,n)\phi_m(x_{a,r})\psi_n(y_{a,r}). \tag{10}$$

The equation for coupling the motions is expressed as

$$\sum_{n=1}^{N}\sum_{m=1}^{M}\left(K_{floor} - M_{floor}\omega^2\right)u_{floor} + \sum_{r=1}^{R} k_{a,r}\left(1+j\eta_{a,r}\right)\left(w_{a,r} - w_{floor,r}\right) = F, \tag{11}$$

$$m_{a,r}\omega^2 w_{a,r} + w_{a,r}\left(1+j\eta_{a,r}\right)\left(w_{floor,r} - w_{a,r}\right) = 0, \quad r = 1,2\ldots R, \tag{12}$$

in which $k_{a.r}$, $m_{a.r}$ and $\eta_{a.r}$ are the spring constant, mass and loss factor of the rth vibration absorbers, and R is the number of the absorbers.

By organizing the properties of the absorbers in a vector form as

$$\mathbf{K_a} = \left[k_{a,1}\left(1+j\eta_{a,1}\right)\ldots\ k_{a,R}\left(1+j\eta_{a,R}\right)\right], \qquad \mathbf{M_a} = \left[m_{a,1}\ldots\ m_{a,R}\right], \tag{13}$$

and defining a coupling matrix

$$\mathbf{\Phi_a} = \left[\ldots\ \mathbf{\Phi_{a,n}}\ \ldots\right], \qquad \mathbf{\Phi_{a,n}} = \left[\phi_m(x_{a,r})\psi_n(y_{a,r})\right]_{R\times M}, \quad m = 1,2\ldots M, \qquad n = 1,2\ldots N, \tag{14}$$

the coupled motion is solved in matrix form as

$$\left(\begin{bmatrix}\mathbf{K}_{floor} & -\mathbf{\Phi_a}^T\mathbf{K_a}\\ -\mathbf{K_a}^T\mathbf{\Phi_a} & diag(\mathbf{K_a})\end{bmatrix} - \begin{bmatrix}\mathbf{M}_{floor} & \mathbf{0}\\ \mathbf{0} & diag(\mathbf{M_a})\end{bmatrix}\right)\begin{bmatrix}\mathbf{u_{floor}}\\ \mathbf{w_a}\end{bmatrix} = \begin{bmatrix}\mathbf{F}\\ \mathbf{0}\end{bmatrix}, \tag{15}$$

where $\mathbf{w_a} = [w_{a,1}\ \ldots\ w_{a,R}]^T$.

4 Results of the measurements and the prediction model

Figure 17 shows the measured mobility of the joist structure with and without vibration absorbers. The mobility values are root-mean-squared averaged among the positions described in Figure 4. From the figures, it can be observed that the absorbers lead to a large change in the structure vibration near 70Hz, while the changes in other frequency ranges are small. Comparing to the impacts far from the absorbers (Figure 17c and 17d), the floor mobility is reduced more significantly when the impact position is close to the area of the absorbers (Figure 17a and 17b). Due to the absorbers' low damping, the vibrational energy at the target structure mode is not much dissipated by the absorbers but rather distributed to the frequency ranges surrounding the target frequency. Thereby two peaks at around 65 and 88 Hz can be observed in the figure. For the other modes of the absorber at 13.7, 33.5, and 115Hz (Figure 8), no significant changes of the mobility were found in the figures.

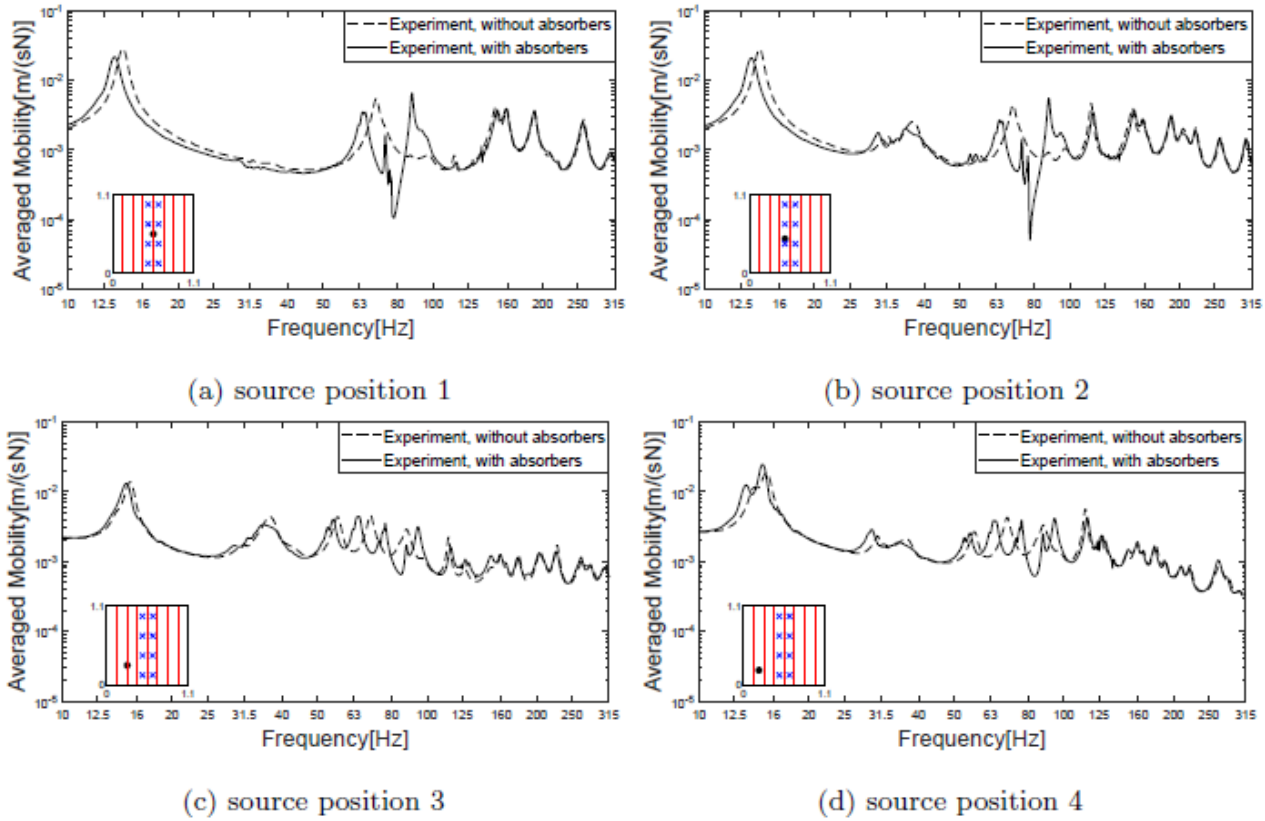

Figure 17 – Averaged mobility of the scaled joist floor with and without vibration absorbers. The small maps show the impact position as ’black dot’ and absorber’s position as ’blue crosses’.

In Figure 18, the MAC values between the experiment and simulation were calculated and compared for the first 18 floor modes (up to about 190 Hz). The values show a reasonable correlation between the measured and predicted results. Figure 19 and 20 display some identified mode shapes of the joist floor. The measured and the predicted modes have similarities in both the mode shapes and the natural frequencies.

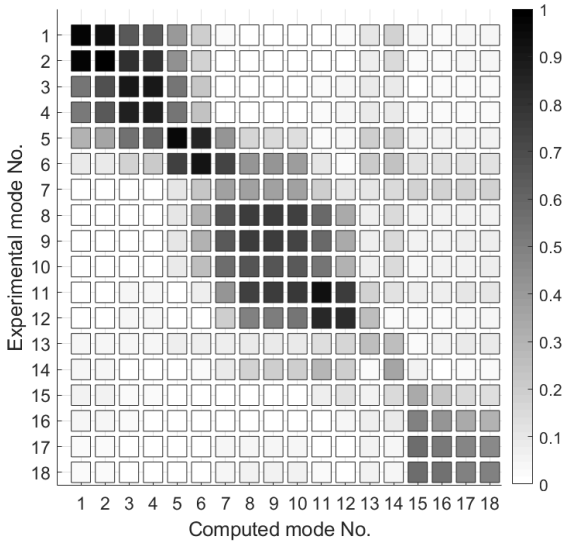

Figure 18 – MAC values between the measurement and the analytical model of the joist structure.

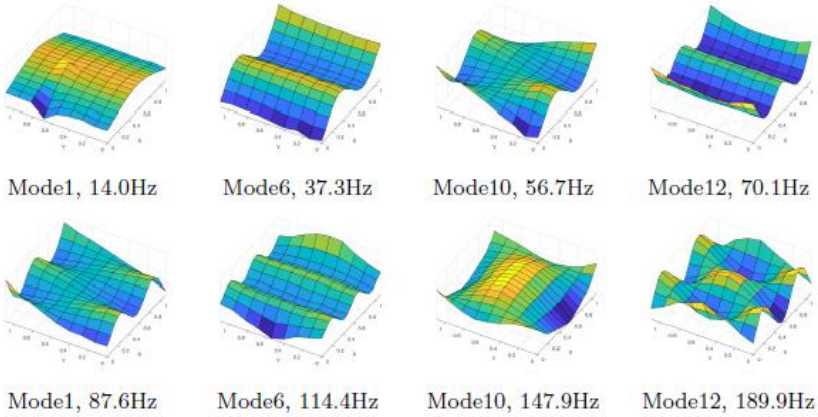

Figure 19 – Measured mode shapes and natural frequencies of the scaled joist floor.

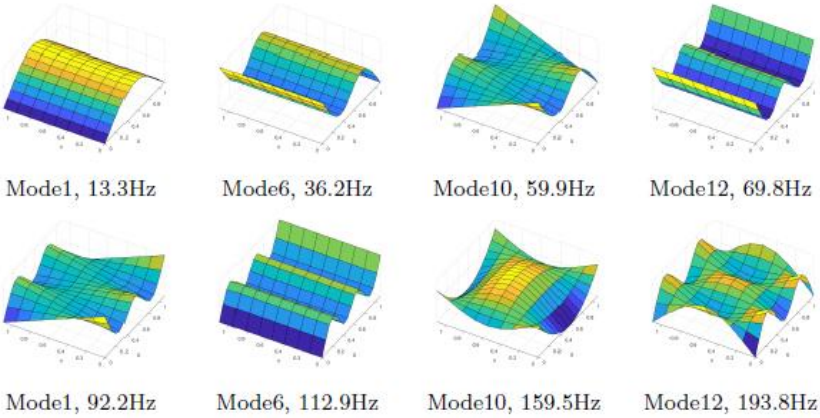

Figure 20 – Simulated mode shapes and natural frequencies of the scaled joist floor.

Comparisons were also made between the mobility of the joist structure with and without the vibration absorbers (Figure 21). In general, the results from the analytical model are in a good consistency with the results from the experiments. When the impact and receiver are located close to the centre of the floor, the results show fewer modes and appear to be more consistent with each other than for scenarios where the distance between excitation and receiver positions is larger.

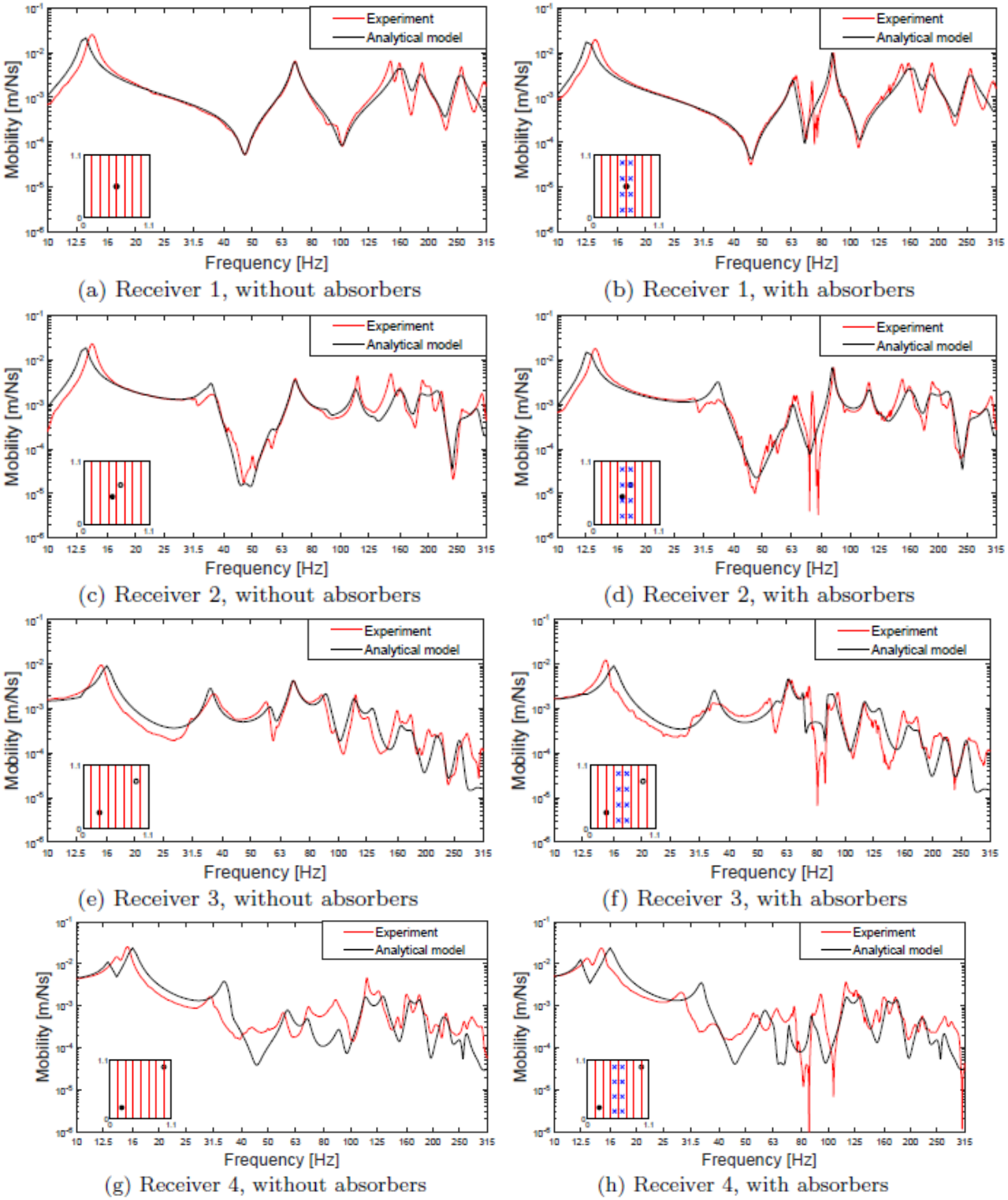

Figure 21 – Mobility of the scaled joist floor. The small maps show excitation position 'black dot', receiver position 'black circle' and vibration absorber's position 'blue crosses'.

The model also gives an accurate prediction of the obvious change in floor vibration pattern around 70 Hz due to the absorbers. As it is difficult to control the fabricated vibration absorbers to have exactly the same natural

frequency, the experimental results show some fluctuations around 70Hz. The vibration absorbers have little effect on frequencies other than those around their natural frequency.

Lastly, the reduction of floor vibration level in one third octave band averaged over all positions was compared between the predictions and measurements, see Figure 22. The predicted result shows a similar trend as the measured result, but still a 3 dB deviation exists between the two results in the 63Hz band. For the lower frequency bands, the level reductions are more sensitive to the single mode due to the narrower bandwidths. For example, in the 16 Hz band, a large reduction in vibration level occurs. Looking at Figure 21, it can be explained by a frequency shift of the mobility when comparing measured and modelled results.

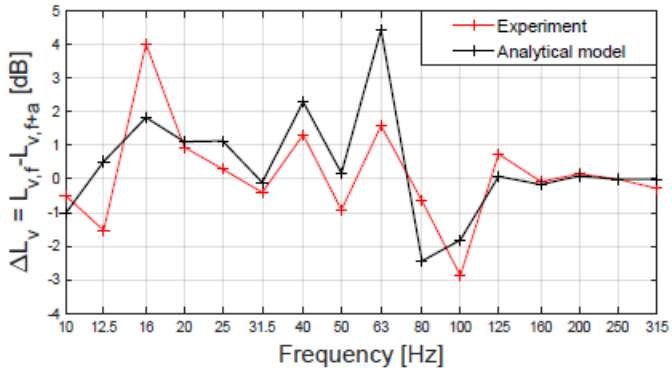

Figure 22 – Reduction of the floor velocity level by the vibration absorbers.

5 Discussion

The experiments in this study were conducted mainly to validate the prediction model. A low loss factor around 0.01 was extracted from the fabricated absorbers. With such a damping value, the absorber can only interfere rather than largely reduce the floor vibration. This is the reason that the measured velocity level reduction is only less than 2dB in 63Hz band in Figure 25. To achieve an effective reduction of the floor vibration and impact sound, safeguarding sufficient damping of the absorber remains a key task.

In the current joist floor model, the revised second moment of inertia does help to approximate the tight connection between the plate and beams. The value of $z'=0.5h_b$ is simply determined as the distance from the neutral plane of the beam to the physical interface between the plate and beam. For different floor boundary conditions or ways of connection between the plate and beams, this value may vary or is dependent on the modes.

The free boundary condition was chosen in the laboratory experiment to verify the applicability of the model for predicting the effect of the multiple SDOF vibration absorbers on the vibration of the lightweight joist floors. The model has been proven to be useful under the free boundary condition. For the other boundary conditions, this model is also expected to be able to achieve the effective predictions when other boundary conditions are applied.

6 Conclusions

In this paper, the effect of multiple vibration absorbers on the floor vibration has been investigated computationally and experimentally.

The impact responses of a freely-supported scaled floor structure with and without vibration absorbers were measured. A mass-spring type of vibration absorber is designed to target the 70Hz mode of the floor. From the measured floor mobility, a significant change was observed near this frequency after the installation of the absorbers. Except for the 70Hz mode, the vibration absorber also has a rotation mode and two swing modes at 14, 34, 115Hz. These modes did not show obvious effects on the floor vibration.

An analytical model of a rectangular ribbed-plate was applied to predict the transfer function of the joist floor influenced by the vibration absorbers. The model assumes the floor as a thin structure and all materials as homogeneous. It is based on the modal superposition method of bending waves and includes the bending and torsional waves in the beams. The vibration absorbers are adapted into the floor mode as multiple SDOF mass-spring systems. In general, the prediction provides a good agreement with the measured result in the frequency range of interest.

References

[1] Gerretsen, E.; Bard, D.; Zhang, B.; Ingelaere, B. *Net-acoustics for timber based lightweight buildings and elements*, COST Action FP0702, 2012.

[2] Bachmann, H.; Ammann, W. J.; Deischl, F.; Eisenmann, J.; Floegl, I.; Hirsch, G. H.; Klein, G. K.; Lande, G. J.; Mahrenholtz, O.; Natke, H. G., et al. *Vibration problems in structures: practical guide-lines*. Birkhauser, 2012.

[3] Sipari, P. Sound insulation of multi-storey houses—a summary of Finnish impact sound insulation results. *Building Acoustics*, 7 (1), 2000, 15–30.

[4] Hopkins, C. *Sound insulation*. Routledge. 2012

[5] Johansson, C. Low-frequency impact sound insulation of a light weight wooden joist floor. *Applied Acoustics*, 44 (2), 1995, 133–147.

[6] Frahm, H. *Device for damping vibrations of bodies*. 1911

[7] Webster, A. C.; Vaicaitis, R. Application of tuned mass dampers to control vibrations of composite floor systems. *Engineering Journal of the American Institute of Steel Construction*, 29 (3), 1992, 116–124.

[8] Wong, W. O. Optimal design of a hysteretic vibration absorber using fixed-points theory. *The Journal of the Acoustical Society of America*, 139 (6), 2016, 3110–3115.

[9] Baader, J., & Fontana, M. Active vibration control of lightweight floor systems. *Procedia engineering*, 199 , 2017, 2772–27

[10] Hwang, J.-S.; Kim, H.; Moon, D.-H.; Park, H.-G. Control of floor vibration and noise using multiple tuned mass dampers. *Noise Control Engineering Journal*, 59 (6), 2011, 652–659.

[11] Salleh, M. M.; Zaman, I. Finite element modelling of fixed-fixed end plate attached with vibration absorber. *ARPN Journal of Engineering and Applied Sciences*, 11 (4), 2016, 2336–2339.

[12] Gardonio, P.; & Zilletti, M. Sweeping tuneable vibration absorbers for low-mid frequencies vibration control. *Journal of Sound and Vibration*, 354, 2015, 1-12.

[13] Shen, Y.; Peng, H.; Li, X.; & Yang, S. Analytically optimal parameters of dynamic vibration absorber with negative stiffness. *Mechanical Systems and Signal Processing*, 85, 2017, 193-203.

[14] Zhu, X.; Chen, Z.; & Jiao, Y. Optimizations of distributed dynamic vibration absorbers for suppressing vibrations in plates. *Journal of Low Frequency Noise, Vibration and Active Control*, 37 (4), 2018, 1188–1200.

[15] Bonsel, J.; Fey, R.; Nijmeijer, H. Application of a dynamic vibration absorber to a piecewise linear beam system. *Nonlinear Dynamics*, 37 (3), 2004, 227–243.

[16] Ljunggren, F.; Agren, A. Development of a new damper to reduce resonant vibrations in lightweight steel joist floors. *Applied Acoustics*, 63 (11), 2002, 1267–1280.

[17] Bucur, V. *Acoustics of wood*. Springer Science & Business Media, 2006.

[18] Fajrin, J.; Zhuge, Y.; Bullen, F.; Wang, H. The structural behavior of hybrid structural insulated panels under pure bending load. *International Journal of Technology*, 8 (5), 2017, 777–788.

[19] Nashif, A. D.; Jones, D. I.; Henderson, J. P. *Vibration damping*. John Wiley & Sons, 1985.

[20] Wu, B. A correction of the half-power bandwidth method for estimating damping. *Archive of Applied Mechanics*, 85 (2), 2015, 315–320.

[21] Gardonio, P.; Elliott, S. *Driving point and transfer mobility matrices for thin plates excited in flexure*. ISVR Technical Report No 277, 1998.

[22] Bishop, R. E. D.; Johnson, D. C. *The mechanics of vibration*. Cambridge University Press, 2011.

[23] Brunskog, J.; Chung, H. Non-diffuseness of vibration fields in ribbed plates. *The Journal of the Acoustical Society of America*, 129 (3), 2011, 1336–1343.

[24] Dickow, K. A.; Brunskog, J.; & Ohlrich, M. Modal density and modal distribution of bending wave vibration fields in ribbed plates. *The Journal of the Acoustical Society of America*, 134 (4), 2013, 2719–2729.

[25] Bedford, A. M.; Liechti, K. M. Mechanics of materials. *Applied Mechanics Reviews*, 55 (3), 2002, 51.

[26] Kane, T. R.; Levinson, D. A. *Dynamics, theory and applications*. McGraw Hill, 1985.